Subwavelength leaky-wave optical nanoantennas: Directive radiation from linear arrays of plasmonic nanoparticles

Xing-Xiang Liu and Andrea Alù*
Department of Electrical and Computer Engineering, The University of Texas at Austin, Austin, Texas 78712, USA
(Received 6 August 2010; published 19 October 2010)

We analyze here the leaky-wave properties of linear arrays of plasmonic nanoparticles. It is shown that such periodic arrays may support two orthogonal leaky-wave propagation regimes, respectively, with longitudinal and transverse polarization. Using closed-form dispersion relations derived in the complex domain, we analyze their properties in the leaky-wave regime and we derive general conditions under which a nanoparticle array with subwavelength lateral cross section may support a radiating leaky mode with directive properties, conical radiation, frequency scanning and sufficiently long propagation distance, paving the way to potential applications as a leaky-wave optical nanoantenna with subdiffractive properties. Realistic designs and configurations are presented, considering the material dispersion and absorption of optical materials, for which we determine propagation distance, near-field distribution and far-field leaky-wave radiation pattern.

DOI: 10.1103/PhysRevB.82.144305 PACS number(s): 78.67.Bf, 42.70.Qs, 42.82.Et, 71.45.Gm

I. INTRODUCTION

The miniaturization of electronic and optical devices is one of the main challenges in modern communications and computer technology. Various concepts and devices, well established in microwave engineering, have been transplanted to optical frequencies, at which the characteristic size and operating wavelength are orders of magnitude smaller and frequency bandwidths are proportionally larger. One successful example is represented by optical nanoantennas,[1–9] which have been inspired in recent years by well-established concepts at radio frequencies.[10] As another example, in microwave technology the electromagnetic properties of periodic structures play a crucial role in several devices. Various periodic structures, such as slot arrays and frequency selective surfaces, are widely applied as antennas and filters. Recent advances in nanotechnology have made possible to extend also these concepts to optical frequencies, where periodic structures, arrays, and nanoscale metamaterials have been recently investigated for a variety of applications.

As one of the interesting applications of periodic arrays at radio frequencies for radiation applications, leaky-wave antennas are a well-established technology that provides directive radiation and frequency beam scanning.[10–12] The recent application of metamaterial concepts has provided novel possibilities for leaky-wave antenna design and operation at microwave frequencies.[13–15] Translating these concepts to the optical domain may open new areas in optical communications, control of radiation and optical computing. In this regard, periodic arrays of nanoparticles have already been considered by various groups as optical waveguides with confined beams, overcoming the optical diffraction limit.[16–25] Dielectric waveguides are generally limited by diffraction to have a transverse cross section comparable with the wavelength, as guided optical beams tend to spread in the background material when the waveguide is too thin.[26] However, the use of plasmonic materials, and arrays of subwavelength plasmonic nanoparticles, in particular,[16–25] may overcome this limitation and confine a guided optical beam over a transverse cross sections significantly smaller than the wavelength, supporting *subdiffractive propagation* with relevant applications in optical computing and communications.

This same nanoparticle array, which is realizable within available nanofabrication technology, may also provide an interesting way of realizing leaky-wave nanoantennas with subwavelength lateral cross section and directive radiation at a specific angle in the far field. Our group has theoretically investigated in the past guided-wave propagation along linear chains of plasmonic and metamaterial particles as optical nanotransmission lines with subdiffractive properties.[27] Our contribution to this problem consisted in the derivation of a closed-form dispersion relation for real and complex dipolar modes supported by such arrays with the only approximation being the neglect of multipoles of higher order than the dominant dipolar contribution from each particle. In particular, this formulation makes it possible to deal with the presence of realistic losses and damping for the guided modes, extending previous analyses that were limited to real wave numbers to the complex domain by an analytic continuation technique.[27] Similarly, this technique may be applied to problems involving radiation losses, coming into play when the wave energy is not totally guided along the particle chain, but partially leaked out, as it happens in leaky modes.

As mentioned above, the idea of energy leakage is widely applied in microwave engineering to design directive radiators with beam scanning capabilities. A leaky mode is a fast eigenmode of the structure with complex wave number, whose real part is less than the free-space wave number.[28] This ensures that the energy is not confined along the array, and the Poynting (power flux) vector points toward the lateral direction. Provided that the imaginary part of the leaky wave number is sufficiently small, the radiation from the chain may become very directive, producing a conical directive beam at a given angle from the array axis. At microwaves, leaky-wave antennas are usually obtained by perturbing a guided wave with periodic defects, as in a periodically loaded microstrip line.[29–31] It is challenging, however, to produce defects within a subwavelength transverse cross section, since in such case they tend to weakly interact with the mode of interest, which is usually weakly confined. This is

another clear symptom of the diffraction limit of guided beams in free space. For this reason, the leaky-wave antenna transverse cross section is usually comparable with the wavelength of operation. In optics, surface plasmons may be able to confine the energy within subwavelength cross sections, and there has been some interest in using energy leakage from thin plasmonic films for near-field microscopy.[32–34]

In this work, stemming from our previous analysis of guided modes along periodic linear arrays of subwavelength nanoparticles, we analyze the potential of this geometry to support leaky waves with directive radiation properties in the optical regime, even in the limit in which it has subwavelength (i.e., not limited by the diffraction limitations mentioned above) lateral cross section, in order to form a *subdiffractive* optical leaky-wave nanoantenna. This may lead to the possibility of connecting distant points of an optical nanocircuit board[35] and creating point-to-point links at the nanoscale. In this context, interest in tailoring the optical radiation from linear and planar arrays of nanoparticles, forming Yagi-Uda nanoantenna arrays[36,37] or planar reflectarrays,[38,39] has been recently discussed in several exciting papers. In the following, we derive relevant design parameters and underline the fundamental and general limitations and challenges to the practical realization of leaky-wave nanoantennas as linear arrays of plasmonic nanoparticles. It should be mentioned that an extensive analysis of the complex modes supported by one-dimensional, two-dimensional, and three-dimensional arrays of magnetodielectric particles has been recently reported,[40] including some aspects of the leaky-wave propagation along subwavelength arrays of dielectric and magnetodielectric spheres with large index of refraction. Our general analysis is focused here on plasmonic nanoparticle arrays, which may ensure the application of these concepts at optical frequencies and may provide inherent advantages associated with their anomalous light interaction.

II. THEORETICAL FORMULATION

Consider an infinite linear array of particles oriented along the z axis, periodically located at $z=Nd$ with d being the center-to-center distance and N being any positive or negative integer, consistent with the geometry analyzed in Ref. 27.

Provided that the nanoparticle size is much smaller than the wavelength of operation, its wave interaction is dominated by the dipolar scattering and each element may be safely modeled as a polarizable dipole, fully characterized by its electric polarizability α_{ee}. As commonly done[41] and consistent with the analytical theory in Ref. 27, if $\mathbf{p}_0=\alpha_{ee}\mathbf{E}_0$ is the dipole moment induced by a local electric field $\mathbf{E}_0$ on the particle at $z=0$, it is possible to derive a self-sustained eigensolution traveling along the array in the form $\mathbf{p}_N=\mathbf{p}_0e^{i\beta Nd}$, under an $e^{-i\omega t}$ time convention. Here, β is the complex propagation factor, fully characterizing its propagation and radiation properties. As reported in several papers on the topic,[17–27] the complete eigenmode spectrum may be split into longitudinal and transverse polarizations, consistent, respectively, with Figs. 1(a) and 1(b). The dispersion relations

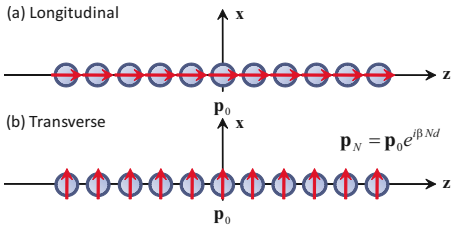

FIG. 1. (Color online) Geometry under consideration: a linear array of polarizable nanoparticles supporting (a) a longitudinal or (b) a transverse eigenmode.

for these two polarizations may be, respectively, written[27]

$$L{:}3\bar{d}^{-3}[f_3(\bar{\beta},\bar{d})-i\bar{d}f_2(\bar{\beta},\bar{d})]=\bar{\alpha}_{ee}^{-1},$$

$$T{:}-\frac{3}{2}\bar{d}^{-3}[f_3(\bar{\beta},\bar{d})-i\bar{d}f_2(\bar{\beta},\bar{d})-\bar{d}^2f_1(\bar{\beta},\bar{d})]=\bar{\alpha}_{ee}^{-1}, \quad (1)$$

where we have introduced the normalized parameters $\bar{d}\equiv k_0d$, $\bar{\beta}\equiv\beta/k_0$, $\bar{\alpha}_{ee}\equiv k_0^3\alpha_{ee}/(6\pi\varepsilon_0)$, $k_0\equiv\omega\sqrt{\varepsilon_0\mu_0}$, and ε_0 and μ_0 are the permittivity and permeability of background medium, respectively. In addition

$$f_N(\bar{\beta},\bar{d})=\mathrm{Li}_N(e^{i(\bar{\beta}+1)\bar{d}})+\mathrm{Li}_N(e^{-i(\bar{\beta}-1)\bar{d}}) \quad (2)$$

and $\mathrm{Li}_N(x)$ is the polylogarithm function, as defined in Ref. 42. Due to the inherent periodicity of the Floquet modes of the linear chain, we limit our analysis to the principal period $|\mathrm{Re}[\bar{\beta}]|\le\pi/\bar{d}$.

The form of dispersion relation Eq. (1) is valid for any real or complex value of β, ensuring that it may be employed to study guided[27] as well as leaky-wave propagation along the linear chains. In our previous work, we have discussed guided propagation along arrays of subwavelength particles, showing that the condition $\mathrm{Im}[\bar{\alpha}_{ee}^{-1}]=-1$ is required for the involved nanoparticles to support a real solution for β (guided modes with no decay).[27] This condition is identically met for passive dipolar particles only when absorption may be neglected,[41,43] as physically expected, and it implies that $\mathrm{Re}[\bar{\beta}]\ge 1$ in Eq. (1). If the lossless condition is not satisfied ($\mathrm{Im}[\bar{\alpha}_{ee}^{-1}]<-1$), then absorption takes place in the nanoparticle array and the eigenwave numbers are necessarily complex, whose imaginary part is associated with the damping caused by Ohmic loss.

Even in the lossless scenario, however, complex solutions are allowed when $|\mathrm{Re}[\bar{\beta}]|<1$ (fast leaky modes), when $1<|\mathrm{Re}[\bar{\beta}]|<\pi/\bar{d}$ (complex modes) or when $|\mathrm{Re}[\bar{\beta}]|=\pi/\bar{d}$ (stop band). In the following, we are interested in leaky modes with sufficiently low $\mathrm{Im}[\bar{\beta}]$, which may provide directive radiation and sustained propagation over a reasonable electrical length, analogous to the operation of microwave leaky-wave antennas.[10] For $\bar{d}<\pi$ (sufficiently tight arrays, which is required for leaky radiation, as we note in the following), the first-order Bloch mode dominates the far-field pattern, which may be therefore evaluated by simply assuming an averaged current line distribution along the z axis with amplitude $-i\omega\mathbf{p}_0e^{i\beta z}/d$, consistent with Ref. 44. In this case,

the magnetic potential $\mathbf{A}$ may be written in the two polarizations as

$$\mathbf{A} = \frac{\omega\mu_0 \mathbf{p}_0}{4d} H_0^{(1)}(\sqrt{k_0^2 - \beta^2}\rho) e^{i\beta z}, \tag{3}$$

where ρ is the radial coordinate in the suitable cylindrical reference system with axis along the cylinder. The electric and magnetic far-field distributions may be easily derived as $\mathbf{H} = \nabla \times \mathbf{A}/\mu_0$, $\mathbf{E} = \nabla \times \mathbf{H}/(-i\omega\varepsilon_0)$.

This implies that a complex value of β necessarily requires a nonzero power flux and phase propagation along the radial direction. In particular, for $\mathrm{Im}[\beta]$ sufficiently small, Eq. (3) represents a standard guided-wave mode for $\mathrm{Re}[\beta] > k_0$ with exponential decay rate in the radial direction given by Ref. 27

$$L: \quad K_1(\sqrt{\mathrm{Re}[\beta]^2 - k_0^2}\rho),$$

$$T: \quad K_2(\sqrt{\mathrm{Re}[\beta]^2 - k_0^2}\rho) \tag{4}$$

and a leaky mode when $\mathrm{Re}[\beta] < k_0$ with conical beam radiation at an angle $\theta = \cos^{-1}[\mathrm{Re}(\bar{\beta})]$ from the z axis. In such case, the decay rate is the one of a cylindrical wave $1/\sqrt{\rho}$ and the corresponding intensity pattern is well approximated by[11]

$$I(\theta) = \frac{\sin^2 \theta}{(\cos \theta - \mathrm{Re}\ \bar{\beta})^2 + (\mathrm{Im}\ \bar{\beta})^2}. \tag{5}$$

The radiation beamwidth of the main conical lobe is calculated as

$$BW = 2\ \mathrm{Im}\ \bar{\beta}/\sin\ \theta_0, \tag{6}$$

which ensures that the *directivity* of radiation, a measure of how oriented and narrow the far-field radiation pattern is toward the desired direction, is inversely proportional to $\mathrm{Im}[\bar{\beta}]$.

It should be emphasized in this context that a complex solution of Eq. (1) implies, in principle, a diverging distribution of the induced dipole distribution along the array, which may raise some questions about the validity of its analytical continuation in the complex domain. It is noticed, however, that similar concerns arise any time we deal with complex eigensolutions of the wave equation, i.e., in regular leaky-wave configurations or even in surface-wave propagation along lossy interfaces. Similar to such cases, this divergence arises only because of the assumption of an infinite array. Leaky-wave solutions do not represent proper contributions to the radiated spectrum of the chain but they indeed dominate the steepest-descent approximation in specific angular regions of the visible spectrum, and therefore they constitute an accurate and effective description of the far-field distribution of the chain in a variety of realistic applications.[10] In practice, their divergence does not constitute an issue, since we are interested in solutions with small $\mathrm{Im}[\beta]$ and finite chain lengths, for which the localized excitation (which may be represented by an emitting molecule or a quantum dot in this scenario at optical frequencies) is at a finite location along the array.[45]

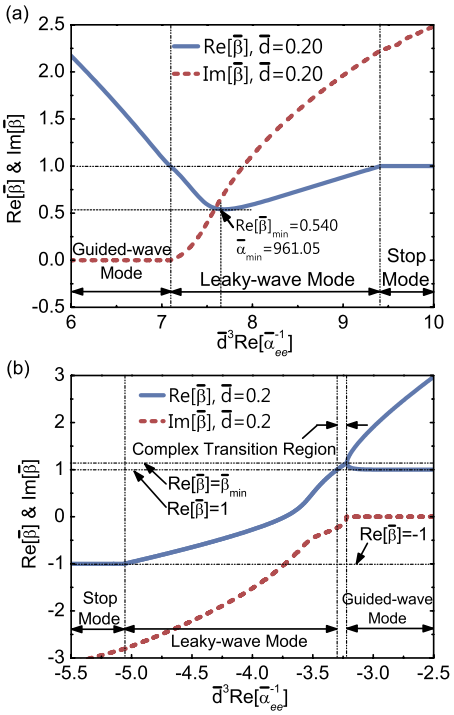

FIG. 2. (Color online) Variation of complex $\bar{\beta}$ in (a) longitudinal and (b) transverse polarization versus the normalized inverse polarizability of the nanoparticles composing the array. Here we consider a normalized center-to-center distance $\bar{d}=0.2$.

III. GENERAL PROPERTIES OF THE LEAKY-WAVE EIGENSOLUTION

In this section, we report our investigation on the general properties of the complex solutions of Eq. (1) with special attention to the leaky-wave regime. In order to make the analysis very general, we focus in this section on the variation in complex $\bar{\beta}$ with the normalized quantity $\mathrm{Re}[\bar{\alpha}_{ee}^{-1}]$, which compactly describes the general properties of the individual nanoparticles forming the array. It is noticed, in particular, that $\mathrm{Im}[\bar{\alpha}_{ee}^{-1}]$ is simply associated with the absorption properties of the particles, and it is forced to be $\mathrm{Im}[\bar{\alpha}_{ee}^{-1}] = -1$ when the particles are lossless. The available degrees of freedom to tailor the leaky-wave properties of the array are therefore compactly represented, to within the dipolar approximation, by $\mathrm{Re}[\bar{\alpha}_{ee}^{-1}]$, which is a function of the geometrical and material properties of the nanoparticles. In the next sections, we will provide specific examples of nanoparticle geometries that may synthesize the required values of $\mathrm{Re}[\bar{\alpha}_{ee}^{-1}]$ obtained in this section.

As a first example, in Fig. 2 we report the variation in complex $\bar{\beta}$ as a function of the normalized parameter $\bar{d}^3\ \mathrm{Re}[\bar{\alpha}_{ee}^{-1}]$, for an interparticle distance $\bar{d}=0.2$. We consider here lossless particles with $\mathrm{Im}[\bar{\alpha}_{ee}^{-1}] = -1$. As seen in Fig. 2(a), the longitudinally polarized eigenmodes have a smooth transition from the guided-wave to the leaky-wave region at $\mathrm{Re}[\bar{\beta}]=1$. The lossless nature of the particles ensures $\mathrm{Im}[\bar{\beta}]=0$ in the guided region $\mathrm{Re}[\bar{\beta}]>1$. As the wave number enters the region $\mathrm{Re}[\bar{\beta}]<1$, the imaginary part starts

increasing, due to the conical radiation of the leaky mode at an angle $\theta_0=\cos^{-1}[\mathrm{Re}[\bar{\beta}]]$. It is recognized that the guided modes in this longitudinal polarization are *inherently forward* in nature, since the slope $\partial\,\mathrm{Re}[\bar{\beta}]/\partial\,\mathrm{Re}[\bar{\alpha}_{ee}^{-1}]$ is negative. As explicitly proven in Ref. 27, in fact, the slope of the curves in Fig. 2 is directly related to whether the modes are forward (negative slope) or backward (positive), which directly determines the sign of $\partial\,\mathrm{Re}[\beta]/\partial\omega$ for passive particles in regions in which $\mathrm{Im}[\bar{\beta}]$ is negligible.

Also in the leaky-wave regime, for low $\mathrm{Im}[\bar{\beta}]$ negative slope is preserved but, for the value $\bar{\alpha}_{ee}^{-1}=\bar{\alpha}_{\min}^{-1}$ the real part of $\bar{\beta}$ reaches a minimum at $\bar{\beta}_{\min}$ and then returns to $\mathrm{Re}[\bar{\beta}]=1$. Similar arguments apply in the low-damping region $\bar{\alpha}_{ee}^{-1}>\bar{\alpha}_{\min}^{-1}$, ensuring that the supported longitudinal leaky-wave modes are forward, *improper*[46] in nature, as also verified by the fact that $\mathrm{Re}[\bar{\beta}]/\mathrm{Im}[\bar{\beta}]>0$, (phase and group velocities are parallel with each other) in the region with small $\mathrm{Im}[\bar{\beta}]$. This follows from the modal dependence $e^{i\beta z}$, which ensures that the phase propagation is in the same direction as the power flow and energy decay, under the condition $\mathrm{Re}[\bar{\beta}]/\mathrm{Im}[\bar{\beta}]>0$.

The level of radiation damping monotonically increases with $\mathrm{Re}[\alpha_{ee}^{-1}]$, implying that the range $\mathrm{Re}[\alpha_{ee}^{-1}]<\alpha_{\min}^{-1}$ is preferable for more directive radiation. This is physically expected, since this is the region closer to the resonance of the individual nanoparticles composing the array, which always arises at $\mathrm{Re}[\alpha_{ee}^{-1}]=0$. Longitudinal leaky modes are inherently supported for positive values of $\mathrm{Re}[\alpha_{ee}^{-1}]$, due to their forward nature, since causality requires[27] $\frac{\partial\,\mathrm{Re}[\alpha_{ee}^{-1}]}{\partial\omega}\leq 0$.

It is worth noticing that the point of minimum $\mathrm{Re}[\bar{\beta}]=\bar{\beta}_{\min}$ arises close to the crossing $\mathrm{Re}[\bar{\beta}]=\mathrm{Im}[\bar{\beta}]$ in the plot of Fig. 2(a). This point may be considered the cut off of the leaky-wave regime, since for $\bar{\alpha}_{ee}^{-1}>\alpha_{\min}^{-1}$ the leaky-wave radiation is damped by rapid longitudinal decay, and its directivity is very limited. The occurrence of a cut off for leaky modes close to where $\mathrm{Re}[\bar{\beta}]=\mathrm{Im}[\bar{\beta}]$ is well known in a variety of leaky-wave antennas,[12] and it is verified in this geometry for different values of $\bar{d}$ in Fig. 3. It is interesting to note that this cut off arises here around the region of minimum $\bar{\beta}$.

In the transverse polarization [Fig. 2(b)], the guided confined branch (right in the figure) is inherently *backward* in nature, since $\partial\,\mathrm{Re}[\bar{\beta}]/\partial\,\mathrm{Re}[\bar{\alpha}_{ee}^{-1}]>0$, due to similar arguments as outlined above, and consistent with analogous findings in thin plasmonic films[47,48] and optical metamaterials.[49] As outlined in Ref. 27, a second, less confined, forward branch is also present in the guided regime, of less interest from the practical point of view, since it is very similar to a plane-wave traveling unperturbed in the background with very limited confinement. A complex branch stems from the contact point between these two guided modes, which enters the leaky-wave regime for sufficiently negative $\mathrm{Re}[\alpha_{ee}^{-1}]$. The dispersion of $\mathrm{Re}[\bar{\beta}]$ with frequency in this regime decreases monotonically from +1 to −1, for decreasing $\mathrm{Re}[\alpha_{ee}^{-1}]$, crossing the axis $\mathrm{Re}[\bar{\beta}]=0$. For this specific value of inverse polarizability, the leaky mode passes from backward *proper*[50]

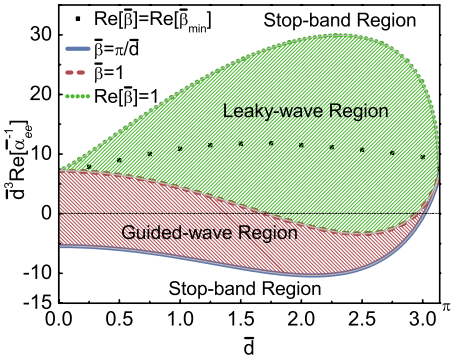

FIG. 3. (Color online) Guided- and leaky-wave regions for longitudinal polarization. The solid blue and dashed red curves are, respectively, the loci of real solutions $\bar{\beta}=\pi/\bar{d}$ and $\bar{\beta}=1$, which delimit the guided-wave regime. The dotted green line defines the upper limit of the leaky-wave regime. The black dots denote the locus $\mathrm{Re}[\bar{\beta}]=\bar{\beta}_{\min}$, which may be considered the cut off of the leaky-wave regime.

(for less negative $\mathrm{Re}[\alpha_{ee}^{-1}]$) to forward *improper* operation. It is evident that in this polarization we are mostly interested in the backward region, which ensures smaller damping factor $\mathrm{Im}[\bar{\beta}]$.

As expected, also in this polarization the most interesting region arises closer to the resonance of the individual nanoparticles, i.e., here for less negative values of $\mathrm{Re}[\alpha_{ee}^{-1}]$. The leaky-wave branch is connected to the guided branches through a complex modal regime, which is typical of a transition between leaky-wave modes and a two-branch guided-wave regime.[12] In this transition region, the mode does not radiate and propagates with complex wave number, whose real part is very close to the one of free space and nonzero imaginary part.

It is interesting to stress that the inherent backward propagation of guided and leaky-wave modes with transverse polarization may be appealing in the framework of negative-index propagation, and this guided regime has been exploited to realize double-negative metamaterials in the visible.[47–49] In terms of leaky-wave radiation, backward radiation may be of interest to increase the degrees of freedom in tailoring and directing the optical radiation but, as we show in the following, it is intrinsically less efficient than the forward longitudinal mode. Farther from resonance, outside the leaky-wave regime, both polarizations have a stop-band region with $|\mathrm{Re}[\bar{\beta}]|=1$, in which the imaginary part grows in magnitude, the propagation is evanescent in nature and the damping is significantly large. In the following, we analyze more in detail the dispersion of the leaky-wave modes as a function of the interparticle distance $\bar{d}$ and of the nanoparticle polarizability with the goal of optimizing the leaky-wave radiation in the two polarizations and of analyzing the fundamental limitations and possibilities of leaky radiation at optical frequencies.

A. Longitudinally polarized modes

Consistent with Fig. 2(a), $\mathrm{Re}[\bar{\beta}]=1$ constitutes the boundary between guided-wave and leaky-wave operation for lon-

gitudinal polarization. Formally, the leaky-wave regime is bounded by the following conditions on the nanoparticle inverse polarizability:

$$\xi(3) + Cl_3(2\bar{d}) + \bar{d}Cl_2(2\bar{d}) < \frac{\bar{d}^3\,\mathrm{Re}[\bar{\alpha}_{ee}^{-1}]}{3} < \mathrm{Re}[f_3(\bar{\beta},\bar{d}) - i\bar{d}f_2(\bar{\beta},\bar{d})]\Big|_{\mathrm{Re}[\bar{\beta}]=1}^{\bar{\beta}\in\mathbb{C}}, \tag{7}$$

where $f_N(\bar{\beta},\bar{d})$ are defined in Eq. (2), $Cl_N(\theta)$ are the Clausen's functions,[42] which are real for real argument and $\zeta(\cdot)$ is the Riemann Zeta function. The left-hand side has been written in closed form using the properties of the polylogarithm functions for real argument

$$Li_1(e^{i\theta}) = Cl_1(\theta) + i\frac{(\pi-\theta)}{2},$$

$$Li_2(e^{i\theta}) = \frac{\pi^2}{6} - \frac{\theta(2\pi-\theta)}{4} + iCl_2(\theta) \quad 0 \le \theta \le 2\pi,$$

$$Li_3(e^{i\theta}) = Cl_3(\theta) + i\frac{\theta(\pi-\theta)(2\pi-\theta)}{12}. \tag{8}$$

Figure 3 shows a map of the different ranges of guided-wave, leaky-wave radiation, or stop band, as a function of $\bar{d}$ and $\mathrm{Re}[\bar{\alpha}_{ee}^{-1}]$. The dashed red line in this plot represents the locus $\bar{\beta}=1$, which separates the guided-wave propagation (below) and leaky-wave radiation (above). The dotted green line represents the upper boundary of the leaky-wave regime, for which $\bar{\beta}\in\mathbb{C}$ and $\mathrm{Re}[\bar{\beta}]=1$. In this plot, we have also considered the locus $\mathrm{Re}[\bar{\beta}_{\min}]$ (black dotted line), which may be considered the cut off for leaky-wave propagation, as discussed above. The solid blue line corresponds to $\bar{\beta}=\pi/\bar{d}$, which is the lower boundary of the guided regime. The regions above the leaky-wave region and below the guided-wave region are stop-band regions, where modes decay very fast along z and are not of interest for guidance or radiation purposes.

It is seen how all the boundary curves converge at $\bar{d}=\pi$ which represents the maximum interparticle distance for supporting guided or leaky mode along arrays of subwavelength nanoparticles. Moreover, the leaky-wave region widens up around $\bar{d}=2$ and it is centered above the resonance condition for the individual nanoparticles $\mathrm{Re}[\bar{\alpha}_{ee}^{-1}]=0$. In the limit $\bar{d}\to 0$, the leaky-wave range Eq. (7) tends to a single point with value $\bar{d}^3\,\mathrm{Re}[\bar{\alpha}_{ee}^{-1}]=6\zeta(3)\simeq 7.21$, implying that too closely packed chains provide a very limited leaky-wave radiation bandwidth.

One of the relevant figures of merit for leaky modes is the ratio $\xi=\mathrm{Re}[\bar{\beta}]/\mathrm{Im}[\bar{\beta}]$. A lower $\mathrm{Re}[\bar{\beta}]$ may be desirable for radiation closer to the normal to the array but this is usually accompanied by a larger $\mathrm{Im}[\bar{\beta}]$, which implies shorter propagation distance and inherently lower directivity. As mentioned above, the cut off of the leaky mode may be defined by $\xi=1$. Overall, a larger value of ξ ensures larger directivity and radiation farther from the array axis, both desirable features of a leaky-wave antenna.

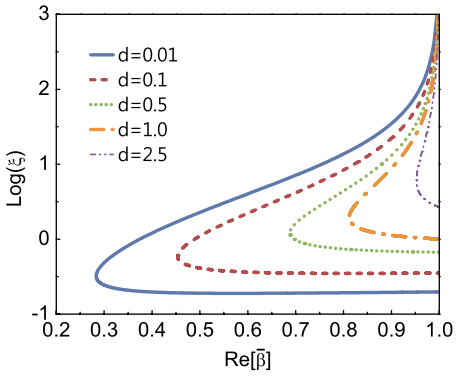

FIG. 4. (Color online) Variation of the ratio $\xi=\mathrm{Re}[\bar{\beta}]/\mathrm{Im}[\bar{\beta}]$ for the supported leaky-wave modes of the nanoparticle chain of Fig. 1 for longitudinal polarization, varying the center-to-center distance.

Figure 4 shows the variation of $\log\xi$ versus $\mathrm{Re}[\bar{\beta}]$ for different values of interparticle distance. The ratio ξ tends to infinity for $\mathrm{Re}[\bar{\beta}]\simeq 1$, since we are operating near the guided-wave regime and lossless particles are being considered here. This region is characterized by endfire radiation, consistent with the limit of a surface mode propagating along the chain. A wider range of $\mathrm{Re}[\bar{\beta}]$ implies that energy may be coupled into a broader angular spectrum, which is more appealing for antenna applications. Figure 4 confirms that better ratios ξ and wider variation along $\mathrm{Re}[\bar{\beta}]$ may be obtained by choosing a smaller value of $\bar{d}$. This is to be expected, since the nanoparticles in this regime are tightly coupled, ensuring more flexibility in terms of guidance and radiation. Consistent with Fig. 2, however, the available bandwidth of leaky-wave operation shrinks down for smaller values of $\bar{d}$. It should be stressed, in addition, that small interparticle distance necessarily requires nanoparticles with smaller diameters, which, in turn, implies higher individual Q factors and more sensitivity to losses. We discuss these aspects in the following section, when we consider specific models for the nanoparticle geometry.

B. Transversely polarized modes

Transversely polarized leaky modes behave quite differently. As discussed above, guided-wave and leaky-wave regions are separated by a complex transition region, not present in the longitudinal polarization. By setting $\mathrm{Re}[\bar{\beta}]=\pm 1$ and solving for the corresponding $\mathrm{Im}[\bar{\beta}]$ in Eq. (1), we can obtain the range of polarizability values that support leaky-wave propagation in this regime. This condition may be formally expressed as

$$[f_3(\bar{\beta},\bar{d}) - i\bar{d}f_2(\bar{\beta},\bar{d}) - \bar{d}^2 f_1(\bar{\beta},\bar{d})]\big|_{\mathrm{Re}[\bar{\beta}]=-1} < -\frac{2}{3}\bar{d}^3\bar{\alpha}_{ee}^{-1} < [f_3(\bar{\beta},\bar{d}) - i\bar{d}f_2(\bar{\beta},\bar{d}) - \bar{d}^2 f_1(\bar{\beta},\bar{d})]\big|_{\mathrm{Re}[\bar{\beta}]=1}, \tag{9}$$

where $f_N(\bar{\beta},\bar{d})$ are defined in Eq. (2).

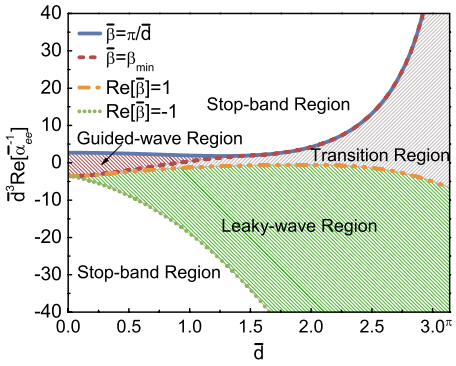

FIG. 5. (Color online) Analogous to Fig. 3, guided- and leaky-wave regions for transversely polarized modes.

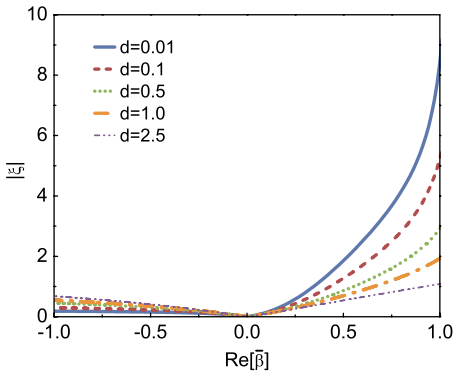

FIG. 6. (Color online) Analogous to Fig. 4, variation in ξ vs $\mathrm{Re}[\bar{\beta}]$ for transversely polarized leaky modes, varying the center-to-center distance.

Figure 5 shows the different modal regions for transversely polarized modes as a function of $\bar{d}$ and $\bar{\alpha}_{ee}^{-1}$, analogous to Fig. 3. Like the longitudinal case, the leaky-wave regime converges to a single point for $\bar{d}\to 0$, implying that also in this polarization the leaky-wave regime is of narrow bandwidth for very tight nanoparticles. On the other extreme, toward $\bar{d}=\pi$, the modal region widens, ensuring a relatively broad range of normalized polarizability values that support leaky modes. As we will point out in the following, however, the corresponding $\mathrm{Im}[\bar{\beta}]$ is rather large for this range of interparticle distance.

Figure 6 shows the variation in ξ with the array properties in this polarization, analogous to Fig. 4. It is evident comparing the two figures that it is more challenging to obtain a reasonably large figure of merit in this polarization. As anticipated earlier, the region of most interest is localized in the backward-wave region, for positive $\mathrm{Re}[\bar{\beta}]$ (right portion of Fig. 6). Due to the presence of a complex transition region between guided-wave and leaky-wave modes, in this polarization the imaginary part $\mathrm{Im}[\bar{\beta}]$ is not negligible even for values $\mathrm{Re}[\bar{\beta}]\simeq 1^{-}$, and the ratio ξ is never remarkably large. These results confirm the general dispersion properties of transverse modes highlighted in Fig. 2(b).

Before concluding this section, it should be mentioned that some of the general modal features highlighted here for linear arrays of nanoparticles may be obtained in thin plasmonic films, in the limit in which the array density increases. This is consistent with recent analyses of complex modes along such geometries,[33] which have also highlighted the presence of backward-wave propagation[47,48] for transverse polarization, consistent with the general results presented here.

IV. REALISTIC MODELS FOR NANOPARTICLES

In the previous section, we have analyzed the general conditions and limitations for leaky-wave propagation along subwavelength nanoparticle chains, considering a general model for the nanoparticle polarizability. In particular, we have shown that longitudinal forward leaky-wave modes may provide better directivity properties than transverse modes, due to their significantly larger value of ξ for the same interparticle distance. Moreover, we have outlined the range of $\mathrm{Re}[\bar{\alpha}_{ee}^{-1}]$ required to sustain leaky-wave radiation. In this section, we will consider realistic nanoparticle geometries to apply the previous general results to several practical designs for optical leaky-wave arrays.

In practice, $\mathrm{Re}[\bar{\alpha}_{ee}^{-1}]$ is determined by the specific design and shape of the nanoparticles forming the array. In the case of spherical nanoparticles of radius a and permittivity ε, for instance, we obtain[27]

$$\mathrm{Re}[\bar{\alpha}_{ee}^{-1}]\simeq \frac{3}{2}(k_0 a)^{-3}\frac{\varepsilon+2\varepsilon_0}{\varepsilon-\varepsilon_0}, \tag{10}$$

in the quasistatic limit of interest here. Other possible geometries of interest may be represented by coated spheres with permittivities ε_1 and ε_2 and ratio of inner to outer radius γ, for which

$$\mathrm{Re}[\bar{\alpha}_{ee}^{-1}]\simeq \frac{3}{2}(k_0 a)^{-3}\frac{2\gamma^3(\varepsilon_2-\varepsilon_1)(\varepsilon_2-\varepsilon_0)-(\varepsilon_1+2\varepsilon_2)(\varepsilon_2+2\varepsilon_0)}{\gamma^3(\varepsilon_2-\varepsilon_1)(2\varepsilon_2+\varepsilon_0)-(\varepsilon_1+2\varepsilon_2)(\varepsilon_2-\varepsilon_0)}, \tag{11}$$

or nanodiscs of radius a, height γa, and permittivity ε, for which the transverse polarizability is[51]

$$\mathrm{Re}[\bar{\alpha}_{ee}^{-1}]\simeq \frac{9}{4}(k_0 a)^{-3}\left[\frac{1}{\gamma}-\frac{1}{(1-\gamma^2)^{3/2}}\left(\frac{\sqrt{1-\gamma^2}}{\gamma}-\arctan\frac{\sqrt{1-\gamma^2}}{\gamma}\right)+\frac{2/\gamma}{\varepsilon/\varepsilon_0-1}\right]. \tag{12}$$

It is evident that there is a wide range of flexibility in the shape and material properties of the nanoparticles to tailor the value of $\mathrm{Re}[\bar{\alpha}_{ee}^{-1}]$ at the frequencies of interest. In the following, we focus on homogeneous nanospheres [Eq. (10)] and analyze how their design parameters affect the leaky-wave dispersion. Analogous results may be derived for different shapes and geometries.

Before analyzing in detail the nanosphere problem, it is relevant to highlight a common trend in the previous formulas (10)–(12): as expected, the value of $\mathrm{Re}[\bar{\alpha}_{ee}^{-1}]$ tends to diverge for small nanoparticles $(k_0 a) \to 0$. This is to be expected, since a small nanoparticle is usually very far from its individual resonance $\mathrm{Re}[\bar{\alpha}_{ee}^{-1}]=0$. On the other hand, leaky-wave radiation requires finite values of $\mathrm{Re}[\bar{\alpha}_{ee}^{-1}]$, as shown in the previous section. This implies that the operation of these leaky-wave nanoantennas with subdiffractive lateral cross section will arise in the frequency range for which the numerator in the right-hand side of Eqs. (10)–(12) is close to zero, i.e., near a plasmonic resonance for the specific shape of interest. For larger $\bar{d}$ this condition becomes more and more stringent, since $\mathrm{Re}[\bar{\alpha}_{ee}^{-1}]$ is required to be closer to zero. This is reflected in a general trade-off between size of these leaky-wave antennas and their bandwidth and robustness to the presence of loss and disorder. We discuss these aspects in further detail, specifically applied to spherical nanoparticles, in the following.

A. Leaky-wave modal dispersion with the nanosphere permittivity

For spherical nanoparticles, we may use Eq. (10) to determine the range of permittivities ε that may allow leaky-wave propagation along the nanoparticle chain. Figure 7(a) shows the longitudinal guided and leaky modal regions in the diagram of $\varepsilon/\varepsilon_0$ vs $\bar{d}$ for different values of the nanosphere radius a. The different curves refer to different ratios $\eta = d/a$ and we have used shadowing to highlight the guided-wave and leaky-wave regions in the case $\eta=3$. As it may be seen, the leaky-wave region requires more negative permittivity values than the guided-wave region, which is centered at the resonance condition of the individual nanospheres $\varepsilon = -2\varepsilon_0$. Denser chains support a wider range of permittivities to achieve leaky-wave propagation, since the permittivity range gets wider for smaller values of η (of course there is a geometrical limit of $\eta > 2$ to consider in the design). This is reflected in wider bandwidths, as negative permittivity is necessarily dispersive with frequency.[52] Consistent with the previous section, in the mathematical limit $\bar{d} \to 0$ leaky waves are not supported, but the permittivity region rapidly widens up for slightly larger values of $\bar{d}$. Figure 7(b) shows the loci of constant $\xi = \mathrm{Re}[\bar{\beta}]/\mathrm{Im}[\bar{\beta}]$ for $\eta=2.2$, as an example. Consistent with the results of the previous section, it is seen that low-attenuation rate is achieved close to the boundary of the guided-wave mode region, corresponding to endfire radiation. However, relatively large values of ξ may be achieved even farther away from the guided-wave regime, which may provide conical radiation off-axis. Moreover, the natural permittivity dispersion of metals may provide frequency scanning for the conical beams radiated by the chain.

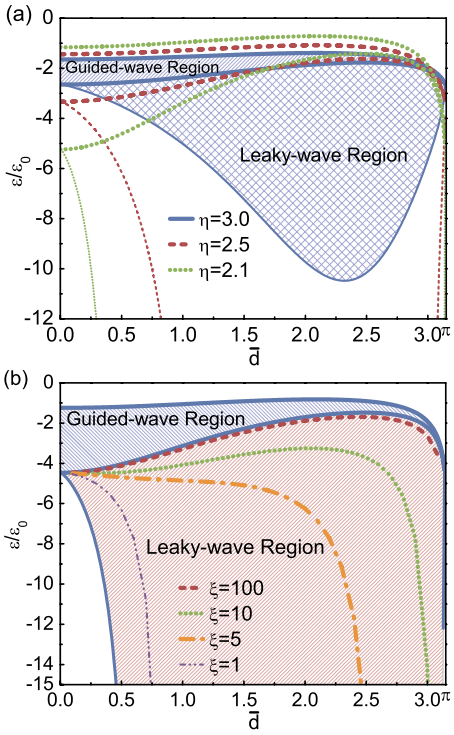

FIG. 7. (Color online) (a) Guided-wave and leaky-wave regions for longitudinal polarization, as a function of nanosphere permittivity and interparticle distance. The guided-wave regime is supported between the bold lines while the leaky-wave region is bounded by thinner lines. (b) Loci of constant $\xi = \mathrm{Re}[\bar{\beta}]/\mathrm{Im}[\bar{\beta}]$ in the leaky-wave region for $\eta=2.2$. Blue solid lines delimit the guided-wave and leaky-wave regions.

Figure 8 shows analogous plots for the transverse polarization. Due to the backward nature of guided and leaky modes in this polarization, less negative values of permittivity are required as compared to the guided regime. Also in this case, by decreasing the value of η the leaky-wave operation broadens in bandwidth. Comparing Figs. 7 and 8, it is seen that longitudinal leaky modes have a broader leaky-wave region and comparatively larger values of ξ, implying that they may outperform the transverse backward-wave leaky modes in terms of directivity and bandwidth of operation. These results are consistent with the discussion in the previous section but applied here specifically to the nanosphere geometry.

B. Effects of absorption and material loss

In this section we relax the assumption that material absorption and losses are negligible in the materials composing the chain, i.e., $\mathrm{Im}[\bar{\alpha}_{ee}^{-1}] < -1$. This is a relevant aspect to consider, since negative permittivity, required to support subdiffractive leaky-wave operation, is usually combined with finite absorption.[52] Material losses are known to play a relevant role in plasmonic devices with subwavelength cross sections, such as nanoparticle waveguides.[27,53,54] In the case of lossy materials, the quasistatic inverse polarizability is related to the complex permittivity $\varepsilon = \varepsilon_r + i\varepsilon_i$ as

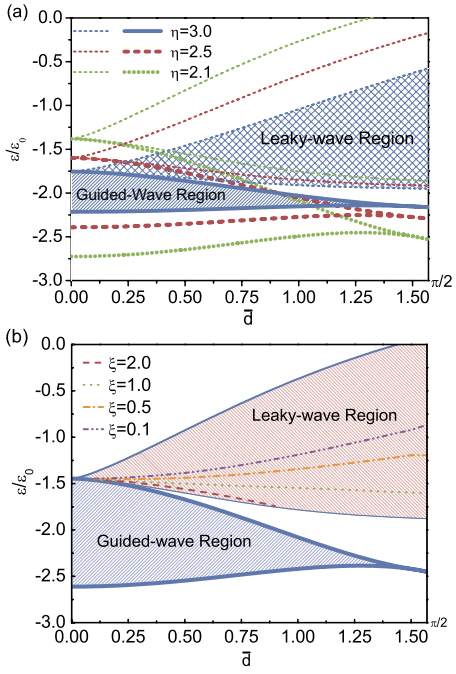

FIG. 8. (Color online) Analogous to Fig. 7, but for transverse polarization.

$$\mathrm{Re}[\bar{\alpha}_{ee}^{-1}] = \frac{3}{2}(k_0 a)^{-3}\frac{(\varepsilon_r + 2\varepsilon_0)(\varepsilon_r - \varepsilon_0) + \varepsilon_i^2}{(\varepsilon_r - \varepsilon_0)^2 + \varepsilon_i^2},$$

$$\mathrm{Im}[\bar{\alpha}_{ee}^{-1}] = -1 - \frac{9}{2}(k_0 a)^{-3}\frac{\varepsilon_0 \varepsilon_i}{(\varepsilon_r - \varepsilon_0)^2 + \varepsilon_i^2}. \quad (13)$$

For low-loss particles, of interest here, ε_i is small and the associated additional contribution to $\mathrm{Im}[\bar{\alpha}_{ee}^{-1}]$ provides a first-order perturbation of the lossless results derived above.

Figure 9 reports the dispersion of $\mathrm{Re}[\bar{\beta}]$ and $\mathrm{Im}[\bar{\beta}]$ versus ε_r for longitudinally polarized modes, for $\bar{d}=0.1$, $\eta=d/a=2.1$, and different levels of material absorption ε_i. It is interesting to see how in the guided-wave region a moderate increase in ε_i principally affects $\mathrm{Im}[\bar{\beta}]$, as expected, but

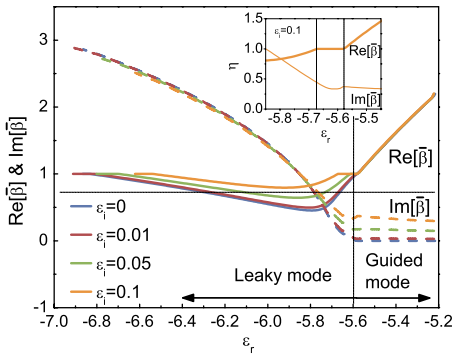

FIG. 9. (Color online) Variation of $\mathrm{Re}[\bar{\beta}]$ and $\mathrm{Im}[\bar{\beta}]$ for $\bar{d}=0.1$ and $\eta=d/a=2.1$ in the longitudinal polarization regime, varying the imaginary part of permittivity. The inset plot shows a zoom in the transition region for the case $\varepsilon_i=0.1$.

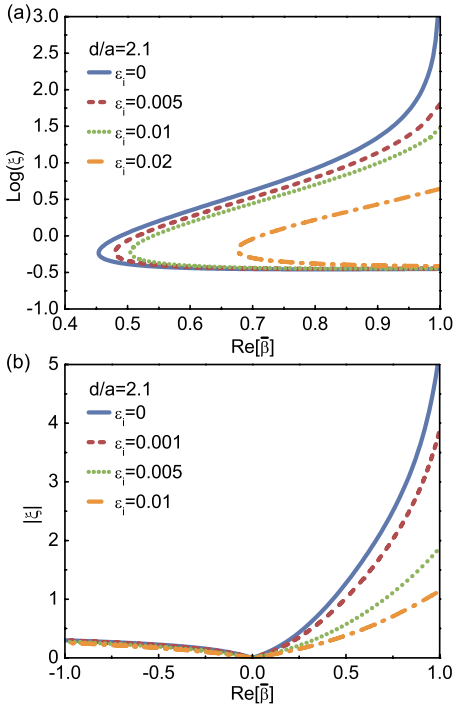

FIG. 10. (Color online) Variation of ξ for different levels of material loss ε_i in (a) longitudinal and (b) transverse polarization. In both plots, we have considered $\eta=d/a=2.1$ and $\bar{d}=0.1$.

leaves unaltered $\mathrm{Re}[\bar{\beta}]$ and correspondingly the phase velocity. Since the transition toward the leaky-wave regime is continuous for this polarization, the presence of material loss implies a reduction in the achievable values of ξ, even near the guided-wave region. In the leaky-wave region, however, the trend is opposite: $\mathrm{Im}[\bar{\beta}]$ is not sensibly altered, being mainly dominated by radiation losses (the mode is less confined to the particles), and the additional small loss mainly affects the angle of radiation and $\mathrm{Re}[\bar{\beta}]$. It is worth noticing that a transition region may arise for relatively larger values of ε_i, for which $\mathrm{Re}[\bar{\beta}]=1$. A zoom of this transition region for $\varepsilon_i=0.1$ is reported in the inset of Fig. 9. The figure confirms that realistic levels of absorption in optical materials may provide the possibility to realize nanoantennas with subdiffractive lateral cross section able to sustain such longitudinal leaky modes with directive radiation properties.

Figure 10 shows the variation in ξ for increased material absorption in the case of $\eta=d/a=2.1$ and $\bar{d}=0.1$, both for (a) longitudinal and (b) transverse polarization. The loss effect is more evident in the longitudinal case, since the transverse polarization has much larger radiation losses. Still, the levels of ξ, and correspondingly of directivity, achieved in the longitudinal polarization remain substantially larger than in the transverse case, even after considering realistic absorption levels.

C. Realistic plasmonic materials

The results of the previous section imply that chains of metamaterial or plasmonic nanoparticles with negative per-

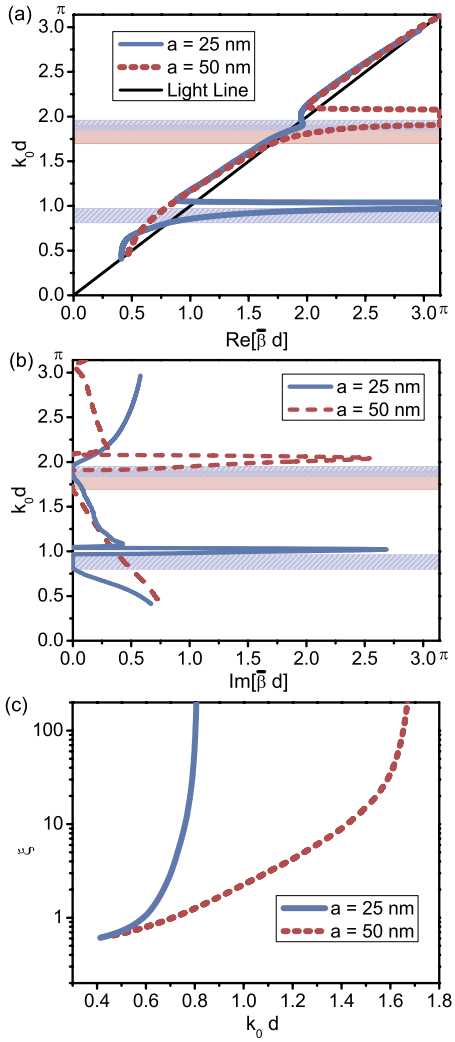

FIG. 11. (Color online) $\bar{\beta}d$ vs k_0d diagrams and ξ for longitudinal modes supported by silver arrays with η=2.1.

mittivity and moderate losses may provide a promising mean to realize a leaky-wave nanoantenna with subwavelength transverse cross section. For this purpose, noble metals, or combinations of noble metals and dielectrics, may be chosen to realize such nanochains, following the design guidelines represented by Eqs. (10)–(12). Metallic nanoparticles made of silver or gold, for instance, have shown moderate guidance properties in the optical regime.[20] In this section, we consider the realistic properties of noble metals in the realization of these nanoantennas. For simplicity, we focus on nanospheres and on longitudinally polarized modes, which ensure better radiation performance and more robustness to the effect of absorption in the materials under consideration.

Figure 11 shows the complex dispersion relations βd-$k_0 d$ for linear arrays composed of silver nanospheres, considering experimental values of permittivity,[55] frequency dispersion and loss. In this case, we have chosen η=2.1 and nanosphere radii of 25 nm (blue solid line) and 50 nm (red dashed). Figure 11(a) reports the real part of βd and Fig. 11(b) the corresponding imaginary part. It is seen that larger particles may provide wider bandwidth of leaky-wave radiation, due to the inherently larger period, and they are inherently more

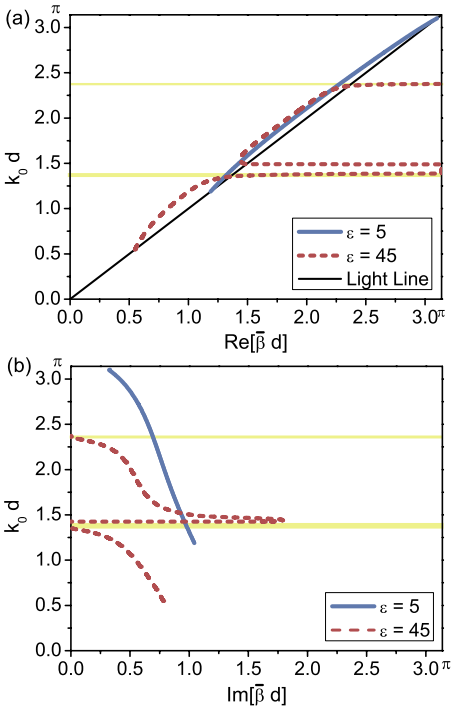

FIG. 12. (Color online) $\bar{\beta}d$ vs k_0d diagrams for longitudinal modes supported by dielectric arrays with η=2.1.

robust to the presence of loss, consistent with analogous results in the guided region.[27] The shadowed regions in the figure indicate these guidance regions. Figure 11(c) reports the calculated values of ξ for the leaky-wave operation. Significantly large values may be achieved near the endfire radiation, despite the presence of loss and the overall subdiffractive lateral cross section of these nanoantennas. These results are particularly encouraging for the realization of these concepts using arrays of subwavelength silver nanoparticles.

D. Comparison with dielectric nanosphere arrays

The previous results imply that plasmonic nanoparticles may represent a promising means for the realization of subdiffractive leaky-wave nanoantennas. In this section we compare their performance with the one of dielectric nanoparticles, focusing in the range $\bar{d}<\pi$. Complex-wave propagation along arrays of spheres with large values of constitutive parameters has been considered in Ref. 40. Figure 12 shows the dispersion of complex modes along a dense array (η=2.1) of dielectric spheres with $\varepsilon=5\varepsilon_0$ and $\varepsilon=45\varepsilon_0$. For consistency with the previous results, we show only guided modes supported by the induced electric dipoles along the array for longitudinal polarization, although for large dielectric constants magnetic modes are also available. Figure 12(a) and 12(b) report the dispersion diagrams for Re[$\bar{\beta}$] and the corresponding Im[$\bar{\beta}$], respectively. For the low permittivity spheres (blue line), guided modes are not available in this low-frequency regime, as expected, and a small complex branch is visible near the light line. Since we are far from resonance, however, the value of ξ is always less

than unity, implying poor radiation properties, as expected. Drastically increasing the nanosphere permittivity it is possible to induce electric-dipole resonances, despite the subwavelength size of the particles. In this situation, guided-wave and leaky-wave regimes are available, and the dispersion diagrams are characterized by narrow guided-wave regions (highlighted by the shadowed regions) connected by leaky-wave branches. In some frequency ranges, significant directivity may be achieved, although the radiation is limited to grazing angles, close to the light line in the diagrams of Fig. 12. It is evident that large permittivity spheres may be also effective in supporting subdiffractive leaky radiation, although the efficiency and directivity values achieved in this example are lower than for plasmonic particles and it may be challenging to realize such large values of permittivity at visible wavelengths. Plasmonic materials with the required values of permittivity, on the contrary, are naturally available at these frequencies, and their dispersion may naturally provide a larger degree of frequency scanning compared to large permittivity materials. We discuss these features further in the next section.

V. FULL-WAVE NUMERICAL SIMULATIONS

In the previous sections, we have used the analytical formulation Eq. (1) to derive the fundamental properties of leaky-wave propagation and radiation along infinite arrays of subwavelength plasmonic nanoparticles to within a dipolar approximation. In this section, we validate the previous analytical model by simulating realistic finite arrays of silver nanoparticles with finite-integration technique commercial software,[56] in order to determine the radiation patterns of such leaky modes in a practical realization, considering also the complete multipolar coupling among closely spaced nanoparticles.

In our numerical simulations, we have fixed the particle size to $a=50$ nm, center-to-center distance $d=110$ nm, and we have used a Drude permittivity model $\varepsilon=\varepsilon_\infty-\frac{f_p^2}{f(f-i\gamma)}$ with $\varepsilon_\infty=5.0$, $f_p=2175$ THz, and $\gamma=4.35$ THz, which describes with good approximation the silver dispersion in the range of frequencies of interest.[57] The overall length of the chain is $L=7$ μm, sufficiently long to ensure that significant part of the power coupled to the leaky mode has been radiated. The array is excited by an optical source (i.e., an emitting molecule or a quantum dot) longitudinally polarized along the array axis to ensure proper coupling with the longitudinal leaky modes supported by the array. We have verified in our simulations that the dispersion of leaky-wave and guided modes along the array is qualitatively consistent with our analytical predictions. Clearly, the nature of our analytical technique neglects higher-order multipolar coupling between the closely spaced nanoparticles, which is reflected in a quantitative difference in the prediction of the frequency range for leaky-wave radiation but qualitatively the results are in good agreement with the previous sections. As an example, Fig. 13(a) reports the normal magnetic field distribution at the operating wavelength $\lambda_0=690$ nm, which is in the leaky-wave regime for this array. Similarly, Fig. 13(b) reports the corresponding distribution at $\lambda_0=600$ nm, for

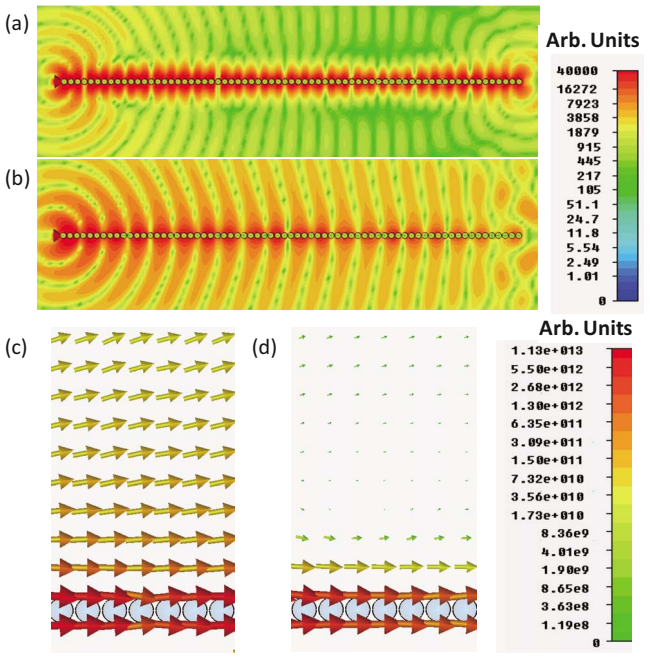

FIG. 13. (Color online) Magnetic field and power-flow distribution for a nanoparticle chain operating in the leaky-wave regime [(a) and (c), at 690 nm wavelength] and in the guided propagation regime [(b) and (d), at 600 nm].

which the chain is in its guided regime. It is evident that the permittivity dispersion of silver allows tuning the guidance properties of the supported mode from a slow mode with short guided wavelength, as in Fig. 13(b), confined along the structure, to a much faster mode, which produces leaky-wave radiation in free space with conical directive properties. The difference in phase velocity between the two simulations is striking, considering that the free-space wavelength difference between the two cases is only 15%, and it is consistent with our analytical theory. Away from the chain, the leaky-wave [Fig. 13(a)] couples to free-space radiation, drastically different from the guided propagation in Fig. 13(b), which decays exponentially far away from the chain axis. The leaky-wave far-field extends laterally and propagates with oblique wave fronts, consistent with the previous analytical results. Figures 13(c) and 13(d) show a zoom in the dashed regions of the two panels of Figs. 13(a) and 13(b), reporting the power-flow (Poynting vector) distribution. The power flow shows significant lateral energy leakage in the leaky-wave scenario of Fig. 13(c). In contrast, at the wavelength $\lambda_0=600$ nm [Fig. 13(d)], the power flow is confined and bounded parallel to the chain, rapidly decaying away from its axis. It is remarkable that these full-wave results qualitatively confirm with very good precision the analytical results in the previous sections, and, in particular, the possibility to create a leaky-wave nanoantenna composed of subwavelength nanoparticles composed of realistic plasmonic materials. The fact that our full-wave results take into account the full coupling among the neighboring particles, and not just their dipolar (dominant) contribution, slightly shifts the guidance and leaky-wave frequency ranges from our analytical predictions in Fig. 11, but qualitatively these results confirm the possibilities noted in the previous sections. Figure 14(a)

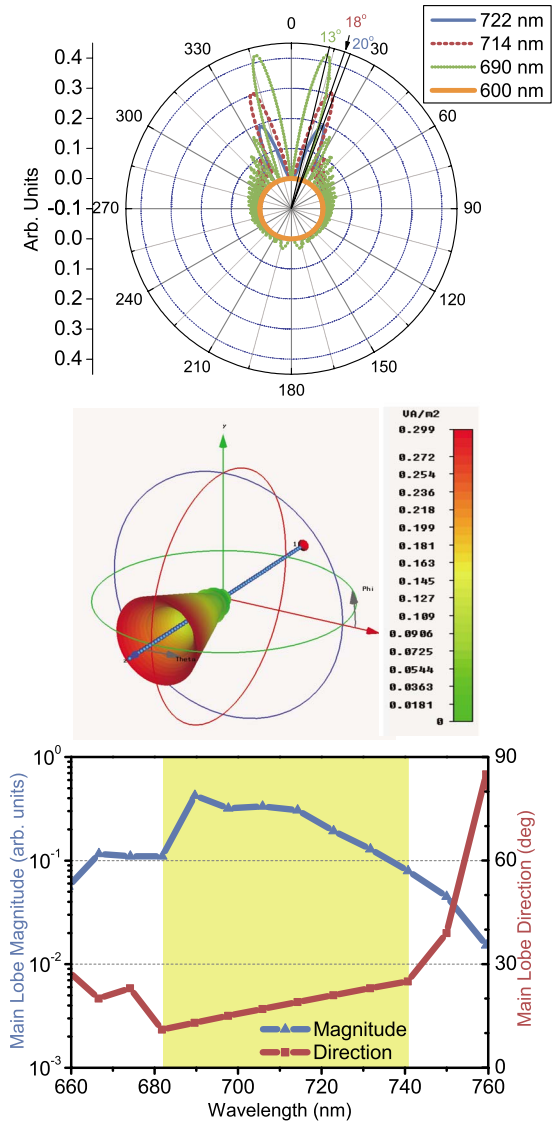

FIG. 14. (Color online) (a) Far-field radiation patterns vs wavelength of operation. At 722 nm (solid blue line), 714 nm (dashed red line), and 690 nm (dotted green line), directional far-field radiation patterns are obtained, pointing at 20°, 18°, and 13°, respectively. At 600 nm, the guided-wave mode does not significantly contribute to the far-field radiation. (b) Calculated three-dimensional leaky-wave radiation pattern at the wavelength of 690 nm. (c) Scanning of the main lobe radiation pattern (magnitude and main direction) versus wavelength. The highlighted region corresponds to leaky-wave operation.

shows the corresponding far-field radiation patterns in the E plane at various wavelengths. It is seen that, in the leaky-wave regime, the conical beam may scan the angle with frequency, as predicted in the previous sections. The patterns show a significant directivity that may be tuned by changing the frequency of operation (i.e., the material permittivity). It is seen that, consistent with the previous analytical results, better directivity is achieved for radiation closer to the chain axis, for which ξ is larger. The scan of the main lobe direction with frequency confirms the forward nature of these longitudinal leaky-wave modes, as predicted by the previous analysis. For comparison, the radiation at $\lambda_0=600$ nm is very poor, due to the guided-wave properties of the chain at this wavelength. The subdiffractive nature and subwavelength period of the chain ensure absence of significant side lobes. These results confirm the realistic possibility of using a silver nanoparticle chain as a leaky-wave nanoantenna. Different nanoparticle size and geometry may be used to tune and shift the leaky-wave operation at different wavelengths. Figure 14(b) reports the three-dimensional far-field radiation pattern at 714 nm, together with the geometry of the chain, to highlight the directive conical radiation at 18° from the chain axis, consistent with Fig. 14(a). Smaller side lobes are visible, associated to the finite length of the chain. As reported in Fig. 14(c), the nanoparticle chain supports a smooth linear scanning region between the wavelengths of 680–740 nm (highlighted in the figure), which delimit the leaky-wave operation of this nanoantenna. Tunability and beam scanning at the same frequency may be envisioned by considering electro-optical materials or proper nonlinearities in the nanoparticles. We will consider these aspects in the near future.

VI. CONCLUSIONS

In this paper, we have provided a detailed analysis of the general leaky-wave radiation properties of linear arrays of subwavelength plasmonic nanoparticles. Using closed-form analytical dispersion relations for real and complex modes supported by such chain, we have analyzed its leaky-mode properties and the most general conditions required to support this regime with large directivity and robust frequency response, in the limit of subwavelength nanoparticles composing the array. In particular, we have shown that the longitudinal polarization is the best candidate for achieving significantly directive conical radiation with scanning capabilities in this regime, and that the transverse polarization may support backward-wave radiation. We have also considered the effects of varying the center-to-center distance, the material properties and the possible presence of material dispersion and loss, specializing our general analysis to realistic plasmonic materials and providing comparison with analogous dielectric arrays. Our analysis shows that plasmonic materials may provide a robust route to leaky-wave radiation at optical frequencies, adding more flexibility over the leaky-wave properties of thin plasmonic films. We have also validated our results with full-wave simulations, analyzing the leaky-wave propagation and radiation along silver nanosphere arrays of finite length. Our full-wave simulations have confirmed that plasmonic leaky-wave nanoantennas with subdiffractive lateral cross section may indeed lie within the realm of current nanotechnology and may be applied to novel devices for optical communications and computing.

ACKNOWLEDGMENTS

The authors are particularly thankful to Robert A. Shore and Nader Engheta for valuable discussions. This work has been supported by the U.S. Air Force Research Laboratory with Contract No. FA8718-09-C-0061.

*Author to whom correspondence should be addressed; alu@mail.utexas.edu

[1] K. B. Crozier, A. Sundaramurthy, G. S. Kino, and C. F. Quate, J. Appl. Phys. **94**, 4632 (2003).

[2] P. J. Schuck, D. P. Fromm, A. Sundaramurthy, G. S. Kino, and W. E. Moerner, Phys. Rev. Lett. **94**, 017402 (2005).

[3] C. E. Talley, J. B. Jackson, C. Oubre, N. K. Grady, C. W. Hollars, S. M. Lane, T. R. Huser, P. Nordlander, and N. J. Halas, Nano Lett. **5**, 1569 (2005).

[4] P. Mühlschlegel, H.-J. Eisler, O. J. F. Martin, B. Hecht, and D. W. Pohl, Science **308**, 1607 (2005).

[5] L. Novotny, Phys. Rev. Lett. **98**, 266802 (2007).

[6] J. B. Lassiter, J. Aizpurua, L. I. Hernandez, D. W. Brandl, I. Romero, S. Lal, J. H. Hafner, P. Nordlander, and N. J. Halas, Nano Lett. **8**, 1212 (2008).

[7] M. Schnell, A. García-Etxarri, A. J. Huber, K. Crozier, J. Aizpurua, and R. Hillenbrand, Nat. Photonics **3**, 287 (2009).

[8] A. Alù and N. Engheta, Phys. Rev. Lett. **101**, 043901 (2008).

[9] A. Alù and N. Engheta, Nat. Photonics **2**, 307 (2008).

[10] R. E. Collin and F. J. Zucker, *Antenna Theory* (McGraw-Hill, New York, 1969).

[11] D. R. Jackson and A. A. Oliner, *Modern Antenna Handbook* (John Wiley & Sons, Hoboken, NJ, 2008), Chap. 7.

[12] P. Lampariello, F. Frezza, and A. A. Oliner, IEEE Trans. Microwave Theory Tech. **38**, 1831 (1990).

[13] A. Lai, T. Itoh, and C. Caloz, IEEE Microw. Mag. **5**, 34 (2004).

[14] L. Lei, C. Caloz, and T. Itoh, Electron. Lett. **38**, 1414 (2002).

[15] L. Sungjoon, C. Caloz, and T. Itoh, IEEE Microw. Wirel. Compon. Lett. **14**, 183 (2004).

[16] S. A. Maier, M. L. Brongersma, P. G. Kik, S. Meltzer, A. A. G. Requicha, and H. A. Atwater, Adv. Mater. **13**, 1501 (2001).

[17] R. A. Shore and A. D. Yaghjian, Electron. Lett. **41**, 578 (2005).

[18] W. H. Weber and G. W. Ford, Phys. Rev. B **70**, 125429 (2004).

[19] R. A. Shore and A. D. Yaghjian, IEICE Trans. Commun. **E88-B**, 2346 (2005).

[20] S. A. Maier, P. G. Kik, H. A. Atwater, S. Meltzer, E. Harel, B. E. Koel, and A. A. G. Requicha, Nature Mater. **2**, 229 (2003).

[21] M. Quinten, A. Leitner, J. R. Krenn, and F. R. Aussenegg, Opt. Lett. **23**, 1331 (1998).

[22] M. L. Brongersma, J. W. Hartman, and H. A. Atwater, Phys. Rev. B **62**, R16356 (2000).

[23] A. L. Aden and M. Kerker, J. Appl. Phys. **22**, 1242 (1951).

[24] J. R. Krenn, M. Salerno, N. Felidj, B. Lamprecht, G. Schider, A. Leitner, F. R. Aussenegg, J. C. Weeber, A. Dereux, and J. P. Goudonnet, J. Microsc. **202**, 122 (2001).

[25] S. A. Maier, P. G. Kik, and H. A. Atwater, Phys. Rev. B **67**, 205402 (2003).

[26] A. Alù and N. Engheta, in *Negative Refraction Metamaterials: Fundamental Properties and Applications*, edited by G. V. Eleftheriades and K. G. Balmain (IEEE Press, Wiley, Hoboken, New Jersey, 2005), Chap. 9, pp. 339–380.

[27] A. Alù and N. Engheta, Phys. Rev. B **74**, 205436 (2006).

[28] J. Hu and C. R. Menyuk, Adv. Opt. Photon. **1**, 58 (2009).

[29] L. Huang, J.-C. Chiao, and M. P. De Lisio, IEEE Trans. Antennas Propag. **48**, 1769 (2000).

[30] P.-W. Chen, C. S. Lee, and V. Nalbandian, IEEE Trans. Antennas Propag. **50**, 832 (2002).

[31] W. Hong, T.-L. Chen, C.-Y. Chang, J.-W. Sheen, and Y.-D. Lin, IEEE Trans. Antennas Propag. **51**, 1922 (2003).

[32] A. Drezet, A. Hohenau, A. L. Stepanov, H. Ditlbacher, B. Steinberger, N. Galler, and F. R. Aussenegg, Appl. Phys. Lett. **89**, 091117 (2006).

[33] J. J. Burke, G. I. Stegeman, and T. Tamir, Phys. Rev. B **33**, 5186 (1986).

[34] A. Bouhelier, Th. Huser, H. Tamaru, H.-J. Guntherodt, and D. W. Pohl, Phys. Rev. B **63**, 155404 (2001).

[35] A. Alù and N. Engheta, Phys. Rev. Lett. **104**, 213902 (2010).

[36] J. Li, A. Salandrino, and N. Engheta, Phys. Rev. B **79**, 195104 (2009).

[37] A. G. Curto, G. Volpe, T. H. Taminiau, M. P. Kreuzer, R. Quidant, and N. F. van Hulst, Science **329**, 930 (2010).

[38] S. Ghadarghadr, Z. Hao, and H. Mosallaei, Opt. Express **17**, 18556 (2009).

[39] A. Ahmadi, S. Ghadarghadr, and H. Mosallaei, Opt. Express **18**, 123 (2010).

[40] R. A. Shore and A. Yaghjian, Air Force Research Laboratory Report No. AFRL-RY-HS-TR-2010-0019, 2010 (unpublished).

[41] S. A. Tretyakov, *Analytical Modeling in Applied Electromagnetics* (Artech House, Boston, MA 2003).

[42] L. Lewin, *Polylogarithms and Associated Functions* (Elsevier, New York, 1981).

[43] J. E. Sipe and J. V. Kranendonk, Phys. Rev. A **9**, 1806 (1974).

[44] S. A. Tretyakov and A. J. Viitanen, Electr. Eng. **82**, 353 (2000).

[45] O. Zhuromskyy, O. Sydoruk, E. Shamonina, and L. Solymar, J. Appl. Phys. **106**, 104908 (2009).

[46] As it follows from the properties of leaky modes (Refs. 10 and 11), these forward modes are inherently improper, since they grow in the transverse direction away from the array axis. Although this would violate the radiation condition for infinite arrays, these eigenmodes indeed dominate the far-field pattern of finite arrays for small $\mathrm{Im}[\bar{\beta}]$.

[47] J. A. Dionne, L. A. Sweatlock, H. A. Atwater, and A. Polman, Phys. Rev. B **72**, 075405 (2005).

[48] A. Hohenau, A. Drezet, M. Weißenbacher, F. R. Aussenegg, and J. R. Krenn, Phys. Rev. B **78**, 155405 (2008).

[49] A. Alù and N. Engheta, Phys. Rev. B **75**, 024304 (2007).

[50] In analogy with Ref. 46 and in agreement with Refs. 10 and 11, these backward modes are inherently proper, since they decay in the transverse direction away from the array axis. These may be considered proper physical eigensolutions of the array even in the limit of infinite geometries.

[51] R. E. Collin, *Field Theory of Guided Waves* (IEEE Press, New York, 1991).

[52] L. D. Landau, E. M. Lifshitz, and L. P. Pitaevskii, *Electrodynamics of Continuous Media* (Butterworth-Heinemann, Oxford, 1982).

[53] S. A. Maier, P. E. Barclay, T. J. Johnson, M. D. Friedman, and O. Painter, Appl. Phys. Lett. **84**, 3990 (2004).

[54] S. A. Maier, P. G. Kik, and H. A. Atwater, Appl. Phys. Lett. **81**, 1714 (2002).

[55] E. Palik, *Handbook of Optical Constants of Solids* (Academic Press, New York, 1985).

[56] CST DESIGN STUDIO™, 2009.

[57] P. B. Johnson and R. W. Christy, Phys. Rev. B **6**, 4370 (1972).